

# NFCDS: A PLUG-AND-PLAY NOISE FREQUENCY-CONTROLLED DIFFUSION SAMPLING STRATEGY FOR IMAGE RESTORATION

Zhen Wang, Hongyi Liu\*, Jianing Li, Zhihui Wei

Nanjing University of Science and Technology, Nanjing, China

## ABSTRACT

Diffusion sampling-based Plug-and-Play (PnP) methods produce images with high perceptual quality but often suffer from reduced data fidelity, primarily due to the noise introduced during reverse diffusion. To address this trade-off, we propose Noise Frequency-Controlled Diffusion Sampling (NFCDS), a spectral modulation mechanism for reverse diffusion noise. We show that the fidelity–perception conflict can be fundamentally understood through noise frequency: low-frequency components induce blur and degrade fidelity, while high-frequency components drive detail generation. Based on this insight, we design a Fourier-domain filter that progressively suppresses low-frequency noise and preserves high-frequency content. This controlled refinement injects a data-consistency prior directly into sampling, enabling fast convergence to results that are both high-fidelity and perceptually convincing—without additional training. As a PnP module, NFCDS seamlessly integrates into existing diffusion-based restoration frameworks and improves the fidelity–perception balance across diverse zero-shot tasks.

**Index Terms**— Diffusion Model, Image Restoration, Plug-and-Play, NFCDS

## 1. INTRODUCTION

Image restoration plays a crucial role in numerous practical applications, aiming to reconstruct a high-quality original image  $\mathbf{x}$  from degraded measurements  $\mathbf{y}$ . The degradation process is commonly modeled as:

$$\mathbf{y} = \mathbf{A}\mathbf{x} + \mathbf{n}, \quad (1)$$

where  $\mathbf{A}$  denotes the degradation operator (e.g., a blur kernel or a downsampling matrix), which is typically non-invertible or ill-conditioned, and  $\mathbf{n} \sim \mathcal{N}(\mathbf{0}, \sigma_y^2 \mathbf{I})$  represents additive white Gaussian noise. Due to the inherent non-uniqueness of solutions and high sensitivity to noise, effective image restoration necessitates the incorporation of suitable prior

This work was supported in part by the National Natural Science Foundation of China under Grant 61971223, in part by the Key Laboratory of Analysis of Mathematical Theory and Modeling of Complex Systems, the Ministry of Industry and Information Technology. Corresponding author: Hongyi Liu.

knowledge to regularize the solution and ensure both stability and physical plausibility.

Traditional model-based methods use handcrafted priors (e.g., total variation (TV)[1] or sparsity[2]), which offer theoretical guarantees but often lack the expressiveness to capture complex image statistics, leading to suboptimal restoration. In contrast, deep learning methods achieve strong performance through data-driven learning[3, 4], however, their real-world applicability is limited by high training costs, reliance on paired data, and poor generalization.

Zero-shot image restoration has gained increasing attention, especially via Plug-and-Play (PnP) methods[5, 6]. These methods embed pre-trained denoisers into iterative optimization to deliver powerful results without task-specific training. Diffusion models[7, 8, 9] provide a powerful generative prior for high-fidelity synthesis and have been successfully integrated into PnP-based restoration[10, 11, 12], significantly enhancing quality.

Current diffusion sampling-based PnP methods enforce data consistency in the reverse diffusion process and re-inject noise at each step to guide restoration along stochastic trajectories. While this enhances texture realism, it often compromises data fidelity—revealing noise’s dual role: aiding detail synthesis while degrading structural accuracy.

Therefore, some works have sought to improve restoration by scheduling noise. However, these methods mainly address forward-process noise scheduling (e.g., cosine in IDDPMPM[13] or SNR-adaptive in Simple Diffusion[14]) or sampling trajectory optimization[15], primarily for unconditional generation, and assume spectrally uniform noise, overlooking frequency-dependent effects critical to image restoration.

- We provide the first frequency-domain analysis of injected noise in diffusion sampling, showing its dual role in restoration: Low-frequency noise degrades data-consistent global structures, while high-frequency noise enhances realistic texture synthesis.
- We propose a Noise Frequency-Controlled Diffusion Sampling (NFCDS) strategy that suppresses low-frequency components in the injected noise via a soft-thresholding mask, effectively mitigating structural drift caused by redundant perturbations.

- Experiments on super-resolution and denoising across a benchmark dataset show that our method, without any additional training, can be directly integrated into existing sampling pipelines and achieves a superior balance between reconstruction fidelity and perceptual quality.

## 2. BACKGROUND

### 2.1. Denoising Diffusion Probabilistic Model

Denoising Diffusion Probabilistic Models (DDPM[7]) generate samples by reversing a forward diffusion process that gradually adds Gaussian noise to a clean image until it becomes a standard Gaussian. This process is a fixed Markov chain over  $T$  timesteps. Due to Gaussian distribution properties, the noisy sample at any timestep  $t$  admits a closed-form expression directly from the original image  $\mathbf{x}_0 \sim p_{\text{data}}$ :

$$\mathbf{x}_t = \sqrt{\bar{\alpha}_t} \mathbf{x}_0 + \sqrt{1 - \bar{\alpha}_t} \boldsymbol{\epsilon}, \quad (2)$$

where  $\boldsymbol{\epsilon} \sim \mathcal{N}(\mathbf{0}, \mathbf{I})$ ,  $\alpha_t = 1 - \beta_t$ ,  $\bar{\alpha}_t = \prod_{i=1}^t \alpha_i$  and  $\{\beta_t\}_{t=1}^T$  is a pre-defined variance schedule satisfying  $0 < \beta_t < 1$ .

During sampling, the reverse process reconstructs data by iteratively denoising from pure noise  $\mathbf{x}_T \sim \mathcal{N}(\mathbf{0}, \mathbf{I})$ . DDPM parameterizes this reverse dynamics using a neural network  $\epsilon_\theta(\mathbf{x}_t, t)$  to predict the noise added at step  $t$ . The update rule for one reverse step in DDPM is:

$$\mathbf{x}_{t-1} = \frac{1}{\sqrt{\alpha_t}} \left( \mathbf{x}_t - \frac{\beta_t}{\sqrt{1 - \bar{\alpha}_t}} \epsilon_\theta(\mathbf{x}_t, t) \right) + \sqrt{\beta_t} \boldsymbol{\epsilon}_t, \quad (3)$$

Further, DDIM[16], as a faster generation scheme, offers more flexible sampling trajectories:

$$\mathbf{x}_{t-1} = \sqrt{\bar{\alpha}_{t-1}} \mathbf{x}_{0|t} + \bar{\sigma}_t \epsilon_\theta(\mathbf{x}_t, t) + \sigma_t \boldsymbol{\epsilon}_t, \quad (4)$$

where  $\boldsymbol{\epsilon}_t \sim \mathcal{N}(\mathbf{0}, \mathbf{I})$  and

$$\bar{\sigma}_t = \sqrt{1 - \bar{\alpha}_{t-1} - \sigma_t^2}, \quad (5)$$

$$\mathbf{x}_{0|t} = \frac{\mathbf{x}_t - \sqrt{1 - \bar{\alpha}_t} \epsilon_\theta(\mathbf{x}_t, t)}{\sqrt{\bar{\alpha}_t}}. \quad (6)$$

$\mathbf{x}_{0|t}$  denotes the estimate of the original image  $\mathbf{x}_0$  given the noisy sample  $\mathbf{x}_t$ , which essentially equates to a single Gaussian denoising step.

Thus, DDIM sampling can be viewed as an alternating denoising and re-noising process, and  $\sigma_t$  controls the trade-off between predicted and random noise at sampling steps.

### 2.2. Restoration via Plug-and-Play Diffusion Models

Traditional model-based methods employ a variational framework that constrains the solution space via a prior-based regularization term on  $\mathbf{x}$ , with the following simplified form:

$$\min_{\mathbf{x}} L(\mathbf{x}) = \underbrace{\ell(\mathbf{x}, \mathbf{y})}_{\text{data fidelity term}} + \underbrace{s(\mathbf{x})}_{\text{prior term}}. \quad (7)$$

The PnP framework offers a flexible approach to image restoration. Unlike traditional model-based methods that design explicit regularizers, PnP decouples data fidelity from prior modeling by plugging in an external denoiser as an implicit prior. Specifically, the framework regards the regularizer  $s(\cdot)$  as a strong denoising operator  $D(\cdot, \sigma_t)$ , alternating data consistency and denoising per iteration. The proximal gradient descent update rule is followed:

$$\begin{cases} \mathbf{x}_{0|t} = \mathcal{D}(\mathbf{x}_t, \sigma_t) \\ \mathbf{x}_{t-1} = \mathbf{x}_{0|t} - \mu_t \nabla_{\mathbf{x}} \ell(\mathbf{x}_{0|t}, \mathbf{y}) \end{cases}. \quad (8)$$

Here,  $\mu_t$  is the step-size, and  $\nabla_{\mathbf{x}} \ell(\mathbf{x}_{0|t}, \mathbf{y})$  enforces the data consistency constraint. This mechanism avoids explicit prior modeling and task-specific retraining, achieving high restoration quality with drastically reduced training overhead.

Sampling-based PnP integrates PnP into diffusion sampling by aligning each update with the model's denoising trajectory, preserving data consistency while following a high-quality generative path for more realistic reconstruction. Its typical update rule is:

$$\begin{cases} \mathbf{x}_{0|t} = \mathcal{D}(\mathbf{x}_t, \sigma_t) = \frac{1}{\sqrt{\bar{\alpha}_t}} (\mathbf{x}_t - \sqrt{1 - \bar{\alpha}_t} \epsilon_\theta(\mathbf{x}_t, t)) \\ \mathbf{x}_{t-1} = \sqrt{\bar{\alpha}_{t-1}} \mathbf{x}_{0|t} - \mu_t \nabla_{\mathbf{x}} \ell(\mathbf{x}_{0|t}, \mathbf{y}) + \bar{\sigma}_t \epsilon_\theta(\mathbf{x}_t, t) + \sigma_t \boldsymbol{\epsilon}_t \end{cases}, \quad (9)$$

where  $\nabla_{\mathbf{x}} \ell(\mathbf{x}_{0|t}, \mathbf{y})$  is the data-fidelity guidance and  $\mu_t$  is the guidance scaling factor.

It can be observed that the core of sampling-based PnP variants lies in injecting noise into the traditional iterative denoising framework to introduce controllable stochasticity and thereby achieve more realistic restoration.

Current mainstream methods, such as DD-NRLG[12] and DiffPIR[10], typically adopt this strategy, differing primarily in the formulation of their data consistency constraints. For instance, in DD-NRLG, the data consistency term is given by:

$$\begin{aligned} \nabla_{\mathbf{x}} \ell(\mathbf{x}_{0|t}, \mathbf{y}) \simeq \\ - \frac{1}{\sqrt{\bar{\alpha}_t}} \mathbf{A}^T \left( \frac{1 - \bar{\alpha}_t}{\bar{\alpha}_t} \mathbf{A} \mathbf{A}^T + \sigma_y^2 \mathbf{I} \right)^{-1} \cdot (\mathbf{y} - \mathbf{A} \mathbf{x}_{0|t}). \end{aligned} \quad (10)$$

Despite their superior visual quality, these methods suffer from substantially lower data fidelity than traditional iterative denoising approaches—a limitation rooted in the sampling-induced stochasticity that our study specifically addresses.

## 3. METHOD

To clarify the perception-fidelity trade-off caused by injected noise, we present a frequency-domain analysis of its role in image generation and DD-NRLG-based image restoration.

Images exhibit a distinct frequency-domain energy distribution: low frequencies dominate smooth regions and global

structure, while high frequencies capture fine details such as edges and textures. Any signal  $\mathbf{I}$  can be decomposed into its low- and high-frequency components:

$$\mathbf{I} = \mathbf{I}^{\text{LF}} + \mathbf{I}^{\text{HF}}. \quad (11)$$

This decomposition can be achieved using frequency-domain transforms such as the Fourier transform.

### 3.1. Role of Injected Noise in Image Generation

In image generation, the clean image  $\mathbf{x}_0$  is completely unknown, and the generative process is entirely noise-driven. The reverse update formula of DDIM is:

$$\mathbf{x}_{t-1} = \sqrt{\bar{\alpha}_{t-1}} \mathbf{x}_{0|t} + \sqrt{1 - \bar{\alpha}_{t-1}} \bar{\epsilon}_{t-1}, \quad (12)$$

where  $\mathbf{x}_{0|t} = \frac{\mathbf{x}_t - \sqrt{1 - \bar{\alpha}_t} \epsilon_\theta(\mathbf{x}_t, t)}{\sqrt{\bar{\alpha}_t}}$  is the current estimate of  $\mathbf{x}_0$ , and  $\bar{\epsilon}_{t-1} = \sqrt{1 - \zeta} \epsilon_\theta(\mathbf{x}_t, t) + \sqrt{\zeta} \epsilon_t$  is a weighted combination of  $\epsilon_\theta(\mathbf{x}_t, t)$  and  $\epsilon_t$ . This is a common variant of the DDIM sampling rule (Eq.(4)) that maintains generation quality while controlling diversity via the parameter  $\zeta \in [0, 1]$ .

By applying frequency-domain decomposition to Eq.(12), we obtain the decoupled form as follows:

$$\begin{aligned} \mathbf{x}_{t-1} = & \underbrace{(\sqrt{\bar{\alpha}_{t-1}} \mathbf{x}_{0|t}^{\text{LF}} + \sqrt{1 - \bar{\alpha}_{t-1}} \bar{\epsilon}_{t-1}^{\text{LF}})}_{\mathbf{x}_{t-1}^{\text{LF}}} \\ & + \underbrace{(\sqrt{\bar{\alpha}_{t-1}} \mathbf{x}_{0|t}^{\text{HF}} + \sqrt{1 - \bar{\alpha}_{t-1}} \bar{\epsilon}_{t-1}^{\text{HF}})}_{\mathbf{x}_{t-1}^{\text{HF}}}. \end{aligned} \quad (13)$$

This formulation explicitly decomposes each sampling step into independent low- and high-frequency updates. Meanwhile, the noise  $\bar{\epsilon}_{t-1}$  is also split into its low-frequency  $\bar{\epsilon}_{t-1}^{\text{LF}}$  and high-frequency  $\bar{\epsilon}_{t-1}^{\text{HF}}$  components, enabling a detailed analysis of each frequency component's role in the generative process.



**Fig. 1.** Role of Low-Frequency Noise in Generation.

We first examine the role of noise low-frequency components. As shown in Fig.1 (top to bottom), three diffusion sampling strategies with respect to low-frequency noise are compared: complete removal, removal after a certain step and full retention. It can be observed that completely removing low-frequency noise (i.e., setting it to zero) renders the evolution deterministic, limiting fine-detail refinement and degrading perceptual realism. Partial removal after an initial period



**Fig. 2.** Role of High-Frequency Noise in Generation.

preserves global structure but leaves fine details underdeveloped. These results indicate that low-frequency noise plays a crucial role in shaping the global structure, particularly during the early stages of the sampling process.

Then we examine high-frequency noise components. As shown in Fig.2(a), completely removing high-frequency noise (i.e., setting  $\bar{\epsilon}_{t-1}^{\text{HF}} = 0$ ) causes generated images to degenerate into semantic-free, uniform blobs. Partial removal after structural stabilization introduces patchy artifacts (Fig.2(b)). This demonstrates that high-frequency noise drives early structural evolution and later refines textures; its absence leads to either structural stagnation or excessive smoothing.

Therefore, in generative tasks, the low-frequency components of noise govern the global structure, while the high-frequency components refine details and textures—low frequencies form the skeleton, and high frequencies provide the flesh. Only by properly leveraging noise across frequency bands can generation achieve both structural coherence and visual realism, yielding high-quality images.

### 3.2. Role of Injected Noise in Image Restoration

In image restoration, the goal is to reconstruct a clean image  $\mathbf{x}_0$  consistent with the given measurement  $\mathbf{y}$ . The corresponding DDIM sampling update equation is:

$$\mathbf{x}_{t-1} = \sqrt{\bar{\alpha}_{t-1}} \mathbf{x}_{0|t} - \mu \nabla_{\mathbf{x}} \ell(\mathbf{x}_{0|t}, \mathbf{y}) + \sqrt{1 - \bar{\alpha}_{t-1}} \bar{\epsilon}_{t-1}, \quad (14)$$

where  $\mu$  is the guidance strength and  $\nabla_{\mathbf{x}} \ell(\mathbf{x}_{0|t}, \mathbf{y})$  is the data consistency constraint.

By applying frequency-domain decomposition to Eq.(14), we obtain the decoupled form as follows:

$$\begin{cases} \mathbf{x}_{t-1} = \mathbf{x}_{t-1}^{\text{LF}} + \mathbf{x}_{t-1}^{\text{HF}} \\ \mathbf{x}_{t-1}^{\text{LF}} = \sqrt{\bar{\alpha}_{t-1}} \mathbf{x}_{0|t}^{\text{LF}} - \mu \nabla_{\mathbf{x}}^{\text{LF}} \ell(\mathbf{x}_{0|t}, \mathbf{y}) + \sqrt{1 - \bar{\alpha}_{t-1}} \bar{\epsilon}_{t-1}^{\text{LF}} \\ \mathbf{x}_{t-1}^{\text{HF}} = \sqrt{\bar{\alpha}_{t-1}} \mathbf{x}_{0|t}^{\text{HF}} - \mu \nabla_{\mathbf{x}}^{\text{HF}} \ell(\mathbf{x}_{0|t}, \mathbf{y}) + \sqrt{1 - \bar{\alpha}_{t-1}} \bar{\epsilon}_{t-1}^{\text{HF}} \end{cases} \quad (15)$$

Let us now examine the roles of different noise components in image restoration tasks. A critical distinction from generation tasks is that in restoration problems—such as deblurring or super-resolution—high-frequency details and textures are significantly attenuated or lost in the degraded observation. Therefore, missing high-frequency information is provided by the diffusion prior in restoration, which is precisely the role of high-frequency component of the injected noise.

As illustrated in Fig.3, the intermediate results of the diffusion process of generation Fig.3(a) and restoration Fig.3(b) are presented. Different from generation, in restoration the initial prediction can accurately recover the global (low-frequency) image structure with the aid of the degraded input, and the errors only at the detail level. This indicates that in restoration, the low-frequency content is strongly constrained by the data-consistency condition.



**Fig. 3.** Intermediate processes of generation and restoration.

Consequently, injecting low-frequency noise introduces unnecessary random perturbations, thereby degrading reconstruction fidelity. In contrast, high-frequency noise constructively contributes to synthesizing realistic textures and fine details. This analysis explains why existing sampling-based PnP methods—though capable of high perceptual quality—often suffer from reduced fidelity. Therefore, it is needed to modulate the noise in the diffusion-based restoration.

### 3.3. Noise Frequency-Controlled Diffusion Sampling

To achieve a better fidelity-perception trade-off in image restoration, we propose a noise frequency-controlled diffusion sampling (NFCDS) strategy. NFCDS modulates the noise spectrum by suppressing the low frequencies and retaining high ones. This selective filtering reduces structural interference without compromising texture and structures during the diffusion.

Specifically, at each sampling step, after applying the data consistency constraint and before re-injecting noise, we modulate the noise  $\bar{\epsilon}_{t-1}$  in the Fourier domain as follows:

$$\bar{\epsilon}'_{t-1} = \text{NFCDS}(\bar{\epsilon}_{t-1}, t) = \mathcal{F}^{-1}(\mathcal{F}(\bar{\epsilon}_{t-1}) \odot \mathcal{M}(t)), \quad (16)$$

where  $\mathcal{F}(\cdot)$ ,  $\mathcal{F}^{-1}(\cdot)$  denote the Fourier and inverse Fourier transform;  $\odot$  represents element-wise multiplication; and  $\mathcal{M}(t)$  is a soft-thresholding mask in the Fourier domain that filters out low-frequency components of the noise:

$$\mathcal{M}(t) = \frac{1}{1 + \exp(-\alpha \cdot (||\omega|| - r(t)))}, \quad (17)$$

where  $\omega = (u, v)$  denotes the frequency-domain coordinates;  $r(t)$  controls the low-frequency suppression radius at each sampling step (here we set  $r(t) = r_{\text{thresh}}$ , a fixed constant requiring hyperparameter tuning); and  $\alpha$  governs the mask's transition steepness near the cutoff frequency—larger  $\alpha$  produces a sharper, near hard-threshold response. Finally,

---

**Algorithm 1** Zero-Shot Image Restoration with Noise Frequency-Controlled Diffusion Sampling

---

**Require:**  $\epsilon_\theta(\cdot, t)$ ,  $\mathbf{T}$ ,  $\mathbf{y}$ ,  $\mathbf{A}$ ,  $\{\bar{\alpha}_t\}$ ,  $\mu$

```

1: Initialize  $\mathbf{x}_T \sim \mathcal{N}(\mathbf{0}, \mathbf{I})$ 
2: for  $t$  from  $T$  to 1 do
3:    $\mathbf{x}_{0|t} = \frac{1}{\sqrt{\bar{\alpha}_t}}(\mathbf{x}_t - \sqrt{1 - \bar{\alpha}_t}\epsilon_\theta(\mathbf{x}_t, t))$ 
4:    $\hat{\mathbf{x}}_{0|t} = \mathbf{x}_{0|t} - \mu \nabla_{\mathbf{x}} \ell(\mathbf{x}_{0|t}, \mathbf{y})$ 
5:    $\epsilon_t \sim \mathcal{N}(\mathbf{0}, \mathbf{I})$ 
6:    $\bar{\epsilon}_{t-1} = \sqrt{1 - \zeta} \epsilon_\theta(\mathbf{x}_t, t) + \sqrt{\zeta} \epsilon_t$ 
7:    $\mathbf{x}_{t-1} = \sqrt{\bar{\alpha}_{t-1}} \hat{\mathbf{x}}_{0|t} + \sqrt{1 - \bar{\alpha}_{t-1}} \text{NFCDS}(\bar{\epsilon}_{t-1}, t)$ 
8: end for
9: return  $\mathbf{x}_0$ 

```

---

Eq.(14) is given by:

$$\mathbf{x}_{t-1} = \sqrt{\bar{\alpha}_{t-1}} \mathbf{x}_{0|t} - \mu \nabla_{\mathbf{x}} \ell(\mathbf{x}_{0|t}, \mathbf{y}) + \sqrt{1 - \bar{\alpha}_{t-1}} \cdot \text{NFCDS} \left( \sqrt{1 - \zeta} \epsilon_\theta(\mathbf{x}_t, t) + \sqrt{\zeta} \epsilon_t, t \right). \quad (18)$$

This frequency-domain control mechanism effectively suppresses detrimental low-frequency perturbations and reduces the number of required sampling steps by making early iterations more effective, thereby accelerating the process. It is broadly applicable to any zero-shot image restoration method that achieves high perceptual quality via noise re-injection, as summarized in Algorithm1.

## 4. EXPERIMENT

We evaluate our method on two zero-shot image restoration tasks—super-resolution and Gaussian denoising—against existing diffusion-based approaches. Using DD-NRLG as the primary baseline with its original parameters to avoid hyperparameter tuning effects, we also compare with mainstream methods including DDRM[17], DDNM[18], and DDPG[11]. The values of  $r_{\text{thresh}}$  and  $\alpha$  for NFCDS applied to DD-NRLG are given in Table 1. All experiments use the publicly available DDPM model pre-trained on CelebA-HQ (256×256).

**Table 1.** The selection of parameters.

Parameters	SRx4		Denoising		
	$\sigma_y = 0$	$\sigma_y = 0.05$	$\sigma_y = 0.1$	$\sigma_y = 0.25$	$\sigma_y = 0.5$
$r_{\text{thresh}}$	35	25	64	35	25
$\alpha$	5	5	5	5	5

Super-resolution uses bicubic downsampling with scale factor 4, under both noise-free and noisy ( $\sigma_y = 0.05$ ) con-

**Table 2.** Quantitative results of two tasks on the CelebA-HQ dataset.

CelebA-HQ		SR $\times 4(\sigma_y = 0.)$			SR $\times 4(\sigma_y = 0.05)$			Denoising( $\sigma_y = 0.1$ )			Denoising( $\sigma_y = 0.25$ )			Denoising( $\sigma_y = 0.5$ )		
Method	NFE	PSNR $\uparrow$	LPIPS $\downarrow$	SSIM $\uparrow$	PSNR $\uparrow$	LPIPS $\downarrow$	SSIM $\uparrow$	PSNR $\uparrow$	LPIPS $\downarrow$	SSIM $\uparrow$	PSNR $\uparrow$	LPIPS $\downarrow$	SSIM $\uparrow$	PSNR $\uparrow$	LPIPS $\downarrow$	SSIM $\uparrow$
DDRM	100	31.98	0.057	<b>0.8848</b>	29.53	<b>0.085</b>	0.8313	33.47	0.054	0.9090	30.39	0.083	0.8613	28.01	0.124	0.8135
DDNM	100	31.96	<b>0.049</b>	0.8811	-	-	-	<b>34.01</b>	0.053	<b>0.9147</b>	<b>30.79</b>	<b>0.079</b>	<b>0.8631</b>	28.19	<b>0.099</b>	0.8147
DDPG	100	31.94	<b>0.051</b>	0.8818	29.57	0.106	<b>0.8329</b>	33.42	0.055	0.8800	28.43	0.168	0.8186	25.47	0.179	0.7651
DD-NRLG	100	<b>32.07</b>	<b>0.049</b>	0.8834	29.37	<b>0.097</b>	0.8237	33.51	<b>0.046</b>	0.9037	30.43	<b>0.079</b>	0.8549	<b>28.20</b>	0.121	0.8162
DD-NRLG	<b>50</b>	31.86	0.062	0.8793	29.15	0.114	0.8172	32.95	0.059	0.8741	29.72	0.089	0.8098	27.34	0.133	0.7693
DD-NRLG + NFCDS	<b>50</b>	<b>32.12</b>	<b>0.051</b>	<b>0.8912</b>	<b>29.70</b>	<b>0.085</b>	<b>0.8387</b>	<b>34.10</b>	<b>0.048</b>	<b>0.9101</b>	<b>31.00</b>	<b>0.072</b>	<b>0.8634</b>	<b>28.60</b>	<b>0.096</b>	<b>0.8215</b>

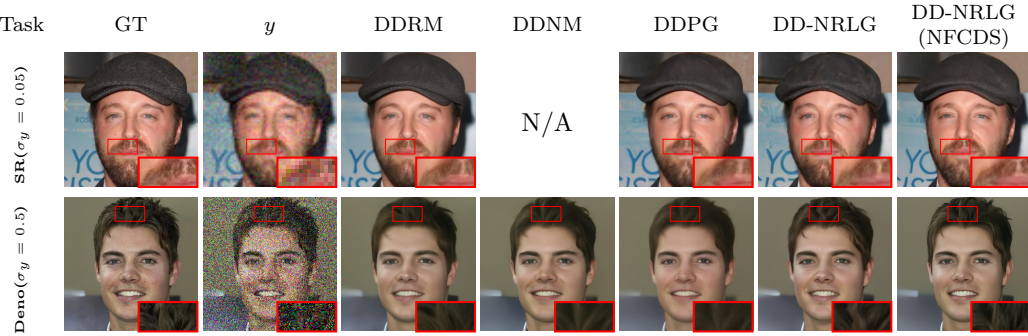


**Fig. 4.** Visual comparison of results (N/A: method is unable to handle the task).

ditions. Gaussian denoising is evaluated at noise levels  $\{0.1, 0.25, 0.5\}$ . Performance is measured by PSNR, LPIPS, and SSIM.

Quantitative results are reported in Table 2. Our method achieves the best or second-best performance in all settings, consistently improving PSNR and SSIM over DD-NRLG while preserving strong LPIPS scores. In noisy super-resolution  $\sigma_y = 0.05$ , the gains in PSNR and SSIM are particularly pronounced, with LPIPS achieving the best value. For denoising under strong noise  $\sigma_y = 0.5$ , integrating NFCDS into DD-NRLG yields a clear improvement: PSNR increases by 0.44 dB and LPIPS decreases by nearly 0.02.

Moreover, we observe that incorporating NFCDS reduces ineffective iterations and significantly lowers the required number of sampling steps, with detailed timing improvements reported in Table 3.

**Table 3.** Inference time comparison.

	NFCDS	NFE	SR	Deno
DD-NRLG	<b>✗</b>	100	8.02s	7.92s
DD-NRLG	<b>✓</b>	50	4.16s	4.12s
Comparison	-	-	<b><math>\downarrow 3.86s</math></b>	<b><math>\downarrow 3.80s</math></b>

The visual comparison as shown in Fig.4 demonstrates that the restoration results, after incorporating the NFCDS mechanism, exhibit more realistic and detailed textures, such as hair and beards. In the super-resolution task, the background is free of the artifacts observed in DD-NRLG.

Furthermore, we conduct super-resolution experiments

**Table 4.** Generalization of NFCDS on DiffPIR and DDPG

CelebA-HQ		SR $\times 4(\sigma_y = 0)$			SR $\times 4(\sigma_y = 0.05)$		
Method		PSNR $\uparrow$	LPIPS $\downarrow$	SSIM $\uparrow$	PSNR $\uparrow$	LPIPS $\downarrow$	SSIM $\uparrow$
DiffPIR		29.83	0.085	0.8352	26.81	0.096	0.7637
DiffPIR + NFCDS		30.02	0.090	0.8458	27.13	0.097	0.7714
DDPG		31.80	0.051	0.8829	29.57	0.106	0.8329
DDPG + NFCDS		32.12	0.062	0.8914	30.01	0.100	0.8412

on both DiffPIR and DDPG to verify the generalizability of NFCDS; quantitative results in Table 4 show that metrics improve significantly after applying NFCDS.

## 5. CONCLUSION

This work addresses the well-known trade-off in sampling-based Plug-and-Play methods, where high perceptual quality is often achieved at the expense of reduced reconstruction fidelity. We analyze the roles of different noise components from a frequency-domain perspective in both generative and restoration tasks, revealing the detrimental impact of low-frequency noise on reconstruction fidelity. Building on this insight, we propose a Noise Frequency-Controlled Diffusion Sampling (NFCDS) strategy that suppresses the low-frequency components of the injected noise in the Fourier domain. Notably, NFCDS requires no additional training and can be seamlessly integrated into existing frameworks, significantly improving reconstruction fidelity while preserving high visual quality.

## 6. REFERENCES

[1] Xueyan Ding, Yafei Wang, Zheng Liang, and Xianping Fu, “A unified total variation method for underwater image enhancement,” *Knowledge-Based Systems*, vol. 255, pp. 109751, 2022.

[2] Jitendra Madarkar, Poonam Sharma, and Rimjhim Padam Singh, “Sparse representation for face recognition: A review paper,” *IET Image Processing*, vol. 15, no. 9, pp. 1825–1844, 2021.

[3] Kai Zhang, Wangmeng Zuo, Yunjin Chen, Deyu Meng, and Lei Zhang, “Beyond a gaussian denoiser: Residual learning of deep cnn for image denoising,” *IEEE Transactions on Image Processing*, vol. 26, no. 7, pp. 3142–3155, 2017.

[4] Zhisheng Lu, Juncheng Li, Hong Liu, Chaoyan Huang, Linlin Zhang, and Tieyong Zeng, “Transformer for single image super-resolution,” in *Proceedings of the IEEE/CVF Conference on Computer Vision and Pattern Recognition(CVPR)*, New Orleans, LA, USA, 2022, pp. 457–466, IEEE.

[5] Singanallur V Venkatakrishnan, Charles A Bouman, and Brendt Wohlberg, “Plug-and-play priors for model based reconstruction,” in *2013 IEEE Global Conference on Signal and Information Processing*, Austin, Texas, USA, 2013, pp. 945–948, IEEE.

[6] Kai Zhang, Yawei Li, Wangmeng Zuo, Lei Zhang, Luc Van Gool, and Radu Timofte, “Plug-and-play image restoration with deep denoiser prior,” *IEEE Transactions on Pattern Analysis and Machine Intelligence*, vol. 44, no. 10, pp. 6360–6376, 2021.

[7] Jonathan Ho, Ajay Jain, and Pieter Abbeel, “Denoising diffusion probabilistic models,” *Advances in Neural Information Processing Systems*, vol. 33, pp. 6840–6851, 2020.

[8] Yang Song and Stefano Ermon, “Generative modeling by estimating gradients of the data distribution,” in *Advances in Neural Information Processing Systems*, Vancouver, Canada, 2019, pp. 11895–11907, MIT Press.

[9] Yang Song, Jascha Sohl-Dickstein, Diederik P Kingma, Abhishek Kumar, Stefano Ermon, and Ben Poole, “Score-based generative modeling through stochastic differential equations,” in *International Conference on Learning Representations*, Vienna, Austria, 2021, pp. 240–275, OpenReview.net.

[10] Yuanzhi Zhu, Kai Zhang, Jingyun Liang, Jiezhang Cao, Bihai Wen, Radu Timofte, and Luc Van Gool, “Denoising diffusion models for plug-and-play image restoration,” in *Proceedings of the IEEE/CVF Conference on Computer Vision and Pattern Recognition(CVPR)*, Vancouver, Canada, 2023, pp. 1219–1229, IEEE.

[11] Tomer Garber and Tom Tirer, “Image restoration by denoising diffusion models with iteratively preconditioned guidance,” in *Proceedings of the IEEE/CVF Conference on Computer Vision and Pattern Recognition(CVPR)*, Seattle, WA, USA, 2024, pp. 25245–25254, IEEE.

[12] Zhen Wang, Hongyi Liu, and Zhihui Wei, “Solving imaging inverse problems via diffusion models with noise-refined likelihood guidance,” in *2025 International Conference on Computer Vision, Image Processing and Computational Photography (CVIP)*, 2025, pp. 211–215.

[13] Alexander Quinn Nichol and Prafulla Dhariwal, “Improved denoising diffusion probabilistic models,” in *International conference on machine learning*. PMLR, 2021, pp. 8162–8171.

[14] Emiel Hoogeboom, Jonathan Heek, and Tim Salimans, “simple diffusion: End-to-end diffusion for high resolution images,” in *International Conference on Machine Learning*. PMLR, 2023, pp. 13213–13232.

[15] Xin Ding, Lei Yu, Xin Li, Zhijun Tu, Hanting Chen, Jie Hu, and Zhibo Chen, “Rass: Improving denoising diffusion samplers with reinforced active sampling scheduler,” in *Proceedings of the Computer Vision and Pattern Recognition Conference(CVPR)*, 2025, pp. 12923–12933.

[16] Jiaming Song, Chenlin Meng, and Stefano Ermon, “Denoising diffusion implicit models,” in *International Conference on Learning Representations*, Vienna, Austria, 2021, pp. 14205–14224, OpenReview.net.

[17] Bahjat Kawar, Michael Elad, Stefano Ermon, and Jiaming Song, “Denoising diffusion restoration models,” *Advances in Neural Information Processing Systems*, vol. 35, pp. 23593–23606, 2022.

[18] Yinhui Wang, Jiwen Yu, and Jian Zhang, “Zero-shot image restoration using denoising diffusion null-space model,” in *International Conference on Learning Representations*, Kigali, Rwanda, 2023, pp. 5402–5432, OpenReview.net.